Traffic 2008; **9:** 910–923
Blackwell Munksgaard

doi: 10.1111/j.1600-0854.2008.00730.x

Ca^{2+} Triggers a Novel Clathrin-Independent but Actin-Dependent Fast Endocytosis in Pancreatic Beta Cells

Zixuan He[1,†], Junmei Fan[2,†], Lijun Kang[2], Jingze Lu[1], Yanhong Xue[1], Pingyong Xu[1], Tao Xu[1,2,*] and Liangyi Chen[1,*]

[1]*National Key Laboratory of Biomacromolecules, Institute of Biophysics, Chinese Academy of Science, Beijing 100101, China*
[2]*Joint Laboratory of Huazhong University of Science and Technology and Institute of Biophysics, College of Life Science and Technology, Huazhong University of Science and Technology, Wuhan 430074, China*
**Corresponding authors: Dr Tao Xu, xutao@ibp.ac.cn and Dr Liangyi Chen, chen_liangyi@yahoo.com*
†*These authors contribute equally to this work.*

The existence of clathrin-independent recycling of secretory vesicles has been controversial. By combining patch-clamp capacitance recording, optical methods and specific molecular interventions, we dissect two types of mechanistically different endocytosis in pancreatic β cells, both of which require GTP and dynamin. The fast one is a novel clathrin-independent but actin-dependent endocytosis that is triggered by high cytoplasmic Ca^{2+} concentration ($[Ca^{2+}]_i$). Large fluorescent dextran (10 nm in diameter) was able to be internalized by this pathway, indicating that it was not likely to be 'kiss and run'. The slow endocytosis is a clathrin-dependent process in which actin plays a complementary role. For the first time, we show that the rate constants for both types of endocytosis exhibit supralinear dependence on increase in $[Ca^{2+}]_i$. Compared with the slow endocytosis, higher $[Ca^{2+}]_i$ level was required to fully accelerate the fast one, indicative of distinct Ca^{2+} sensors for different endocytosis. In the end, we show that physiologically relevant stimulation induces clathrin-independent endocytosis in intact β cells, implying that it may contribute to the normal recycling of secretory vesicles *in vivo*.

Key words: actin, $[Ca^{2+}]_i$, clathrin-independent endocytosis

Received 4 September 2007, revised and accepted for publication 25 February 2008, uncorrected manuscript published online 27 February 2008, published online 19 March 2008

In neurons and endocrine cells, the plasma membrane is retrieved following stimulation-triggered exocytosis to maintain a constant pool of release-competent vesicles. The importance of this endocytic process is highlighted by the fact that blocking vesicle recycling with the *Shibire* (dynamin) mutant in fruit flies leads to immediate paralysis of the animal (1,2). These excitable cells usually exhibit two kinetically distinct forms of endocytosis, a fast one with time constant ranging from 0.1 to 1 second and a slow one that lasts much longer (10–300 seconds) (1,2). Slow membrane retrieval is believed to be a clathrin-mediated process (3,4), while the identity of the fast endocytosis remains controversial. It is proposed to be either a 'kiss and run' (5,6) or a bulk membrane retrieval mechanism (2,7,8).

Another intriguing question is the role of cytoplasmic Ca^{2+} concentration ($[Ca^{2+}]_i$) in the recycling of secretory vesicles. High $[Ca^{2+}]_i$ is reported to either inhibit (9,10) or do not affect endocytosis (11). Conversely, increase in $[Ca^{2+}]_i$ may trigger a fast mode of endocytosis in retinal bipolar neuron (12) and is also found to facilitate endocytosis in a variety of other cell types recently (13–17). Nevertheless, increased stimulation consistently inhibits rather than promotes fast endocytosis in neurons in spite of enhanced elevation in $[Ca^{2+}]_i$ (2), arguing against a simple stimulatory role of $[Ca^{2+}]_i$ in endocytosis. Moreover, it is not known whether or how different types of endocytosis are differentially modulated by the same increase in $[Ca^{2+}]_i$. Therefore, we believe that a clean molecular dissection of distinct vesicle recycling pathways is required to address such questions.

Fusion of secretory vesicles or fission of endocytic vesicles leads to either increase or reduction in the total area of the plasma membrane, which is linearly correlated with the membrane capacitance determined using Lindau–Neher's technique (18). Despite the limitation of measuring only the net changes in membrane surface area, capacitance measurement offers higher temporal resolution than other optical and cell biological methods, and it has been used to monitor vesicle fusion and fission in many types of excitable cells, including pancreatic β cells (19). Pancreatic β cells are a type of endocrine cell that releases insulin in response to food uptake and blood glucose elevation (20). Both depolarization and a homogenous $[Ca^{2+}]_i$ elevation through ultraviolet (UV) photolysis of a caged Ca^{2+} compound induce excessive fast and slow components of membrane capacitance decay in these cells (21,22). The precise molecular mechanisms underlying the fast and the slow membrane retrieval processes are not known. Therefore, we use primary mouse pancreatic β cells and insulin-secreting INS-1 cells and follow the fast and slow components of membrane capacitance decay after homogenously elevating $[Ca^{2+}]_i$ by controlled UV photolysis of 1-(4, 5-dimethoxy-2-nitrophenyl)-1,2-diaminoethane-*N*,*N*, *N*′,*N*′-

tetraacetic acid (DMNP-EDTA). We find that the slow capacitance decay is regulated by clathrin, while the fast one represents a novel clathrin-independent but actin-dependent endocytosis. Both types of endocytosis are positively modulated by $[Ca^{2+}]_i$, and their rate constants are differentially dependent on $[Ca^{2+}]_i$ elevation. In the end, we demonstrate that physiological relevant stimulation triggers both types of endocytosis *in vivo*, as observed using total internal reflection fluorescence (TIRF) microscopy.

Results

Fast and slow endocytosis are differentially regulated by $[Ca^{2+}]_i$

Homogenously elevating $[Ca^{2+}]_i$ to a high concentration (>10 μM) by controlled photolysis led to different responses in membrane capacitance in primary mouse β cells. About 11% (6 out of 56 cells; Table 1) of the cells showed a continuous capacitance increase during uncaging (Figure1A, left), while the majority of cells exhibited one or two components of capacitance decay shortly (0.3–1 second; Supplementary Materials, Table S1) after exocytosis (Figure 1A, middle and right). Similar decays in capacitance were also obtained in insulin-secreting INS-1 cells (Table 1). Shown as an example, we fitted the capacitance decay in Figure 1B with a double exponential function to obtain amplitudes and time constants for different endocytic components. As summarized in Table 1, the averaged time constants and amplitudes for fast and slow endocytosis in INS-1 cells were 0.48 second and 445 fF and 5.11 second and 200 fF, respectively, which were in the same range to those in primary β cells. In addition, glucose elevation consistently induced $[Ca^{2+}]_i$ oscillations in INS-1 cells (Figure S1), implying that these cells were physiologically functional. Because INS-1 cells can easily be manipulated at the molecular level, we used them to investigate the underlying mechanisms of fast and slow endocytosis.

Firstly, we found that enhanced elevation in $[Ca^{2+}]_i$ (from ~10 to ~20 μM) significantly increased the percentage of INS-1 cells showing fast endocytosis (from 36%, $n = 36$, to 63%, $n = 141$), indicating that the fast endocytic process was directly triggered by high $[Ca^{2+}]_i$. Moreover, in cells exhibiting fast endocytosis, the pooled rate of precedent exocytosis was more than twice as fast as cells showing little or slow endocytosis at the same post-flash $[Ca^{2+}]_i$ elevation (Figure 1C). This implies that the fast membrane retrieval is correlated with the precedent rapid fusion of vesicles.

Increase in $[Ca^{2+}]_i$ altered kinetics of both fast and slow retrievals as well. While the amplitude of fast endocytosis (A_{fast}) exhibited no dependence on Ca^{2+} concentration, slow endocytosis (A_{slow}) was linearly correlated with an increase in $[Ca^{2+}]_i$ (Figure S2A,B). On the contrary, both endocytic processes abruptly accelerated as post-flash Ca^{2+} approached certain levels. The endocytic rate constants (r_{fast} and r_{slow}) were calculated as reciprocals of time constants inferred from exponential fits. Their supralinear dependences on $[Ca^{2+}]_i$ could be fitted with Hill equations, which yielded K_d and coefficients (n) of 32 ± 3.2 μM and 4.4 and 23.7 ± 2.5 μM and 7 for rapid and slow endocytosis, respectively (Figure1D). Typically, a Hill equation is used for chemical reactions whose detailed intermediate steps are not known but for which co-operative behavior is suspected, and the coefficient n usually suggests that the reaction is an n-step process (23). Because the Hill coefficient for slow endocytosis is larger than the one for fast endocytosis, it is possible that slow endocytosis is modulated by more Ca^{2+}-dependent processes compared with the fast one. In fact, calcium-dependent phosphatase calcineurin was suggested to participate only in slow endocytosis of chromaffin and neuronal cells (24,25) but not in fast endocytosis of corticotrophs (26). Overall, we conclude that fast and slow endocytosis have different Ca^{2+} sensors; higher $[Ca^{2+}]_i$ is needed to both activate and accelerate the fast membrane retrieval compared with the slow one, while the amplitude of the slow endocytosis but not the fast one is positively modulated by an increase in $[Ca^{2+}]_i$.

Slow endocytosis is clathrin dependent and fast endocytosis is clathrin independent

It is not known yet whether clathrin-dependent endocytosis contributes to the recycling of secretory vesicles in insulin-secreting cells. Therefore, we addressed this question in INS-1 cells by specific molecular manipulations. Epidermal growth factor receptor (EGFR) pathway substrate

Table 1: Percentage of primary β cells and INS-1 cells exhibiting Ca^{2+}-evoked fast, slow and no endocytosis[a]

	Cell number	$[Ca^{2+}]_i$ (μM)	Percentage (fast endocytosis only) (%)	Percentage (slow endocytosis only) (%)	Percentage (both fast and slow endocytosis) (%)	Percentage (no endocytosis) (%)	A_{fast} (fF)	A_{slow} (fF)	τ_{fast} (seconds)	τ_{slow} (seconds)
Pancreatic β cells	56	17 ± 0.9	41	12	36	11	506 ± 52	139 ± 18	0.20 ± 0.02	3.29 ± 0.41
INS-1 cells	253	19 ± 0.3	7	24	53	16	445 ± 31	200 ± 81	0.48 ± 0.02	5.11 ± 0.20

[a]Averaged amplitude and time constants of fast and slow endocytosis are also shown.

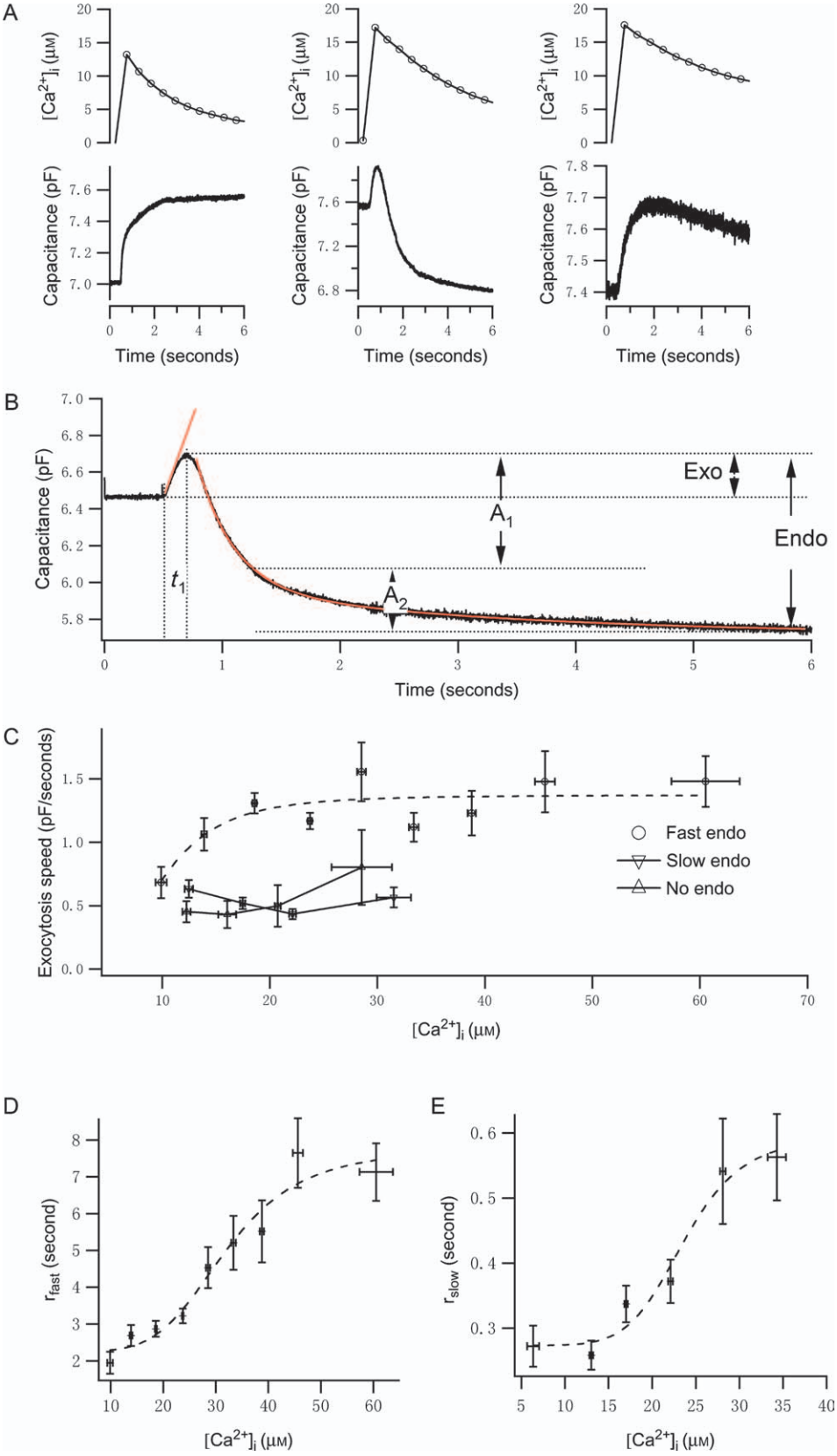

Figure 1: Legend on next page.

clone 15 (Eps15) is an established component of clathrin-coated pits that is ubiquitously and constitutively associated with adaptor protein (AP)-2 or AP-180 in neurons (27), and expression of dominant-negative Eps15 selectively inhibits clathrin-mediated endocytosis (28). Both Ca^{2+}-evoked exocytosis and endocytosis were inhibited in INS-1 cells overexpressing a dominant-negative Eps15 mutant [enhanced green fluorescent protein (EGFP)-EΔ95/295, $n = 30$] but were unaffected in cells expressing the control vector (EGFP-D3Δ2, $n = 19$) (Figure 2). Because amplitudes of both the fast and the slow endocytic components were linearly correlated with amplitudes of precedent exocytosis in the same cells (Figure S2A,B), we divided them by that of the corresponding exocytosis throughout the study to minimize influences of exocytotic fluctuations on endocytosis. After normalization, it was obvious that expressing the dominant-negative mutant led to a selective attenuation of the slow component ($24 \pm 4\%$ of the control, $p < 0.001$), while leaving fast endocytosis relatively intact ($81 \pm 14\%$ of the control, $p = 0.43$). Expressing another dominant-negative Eps15 mutant (DIII) yielded similar results (data not shown). Taken together, these results suggest that the slow retrieval is likely to be a clathrin-dependent process.

Because overexpressing EGFP-EΔ95/295 led to a significant attenuation of exocytosis, we hence directly evaluated the role of clathrin in endocytosis by transfecting cells with short hairpin RNA (shRNA) against the heavy chain of clathrin. A knock-down of clathrin in INS-1 cells was evident, as confirmed by Western blotting shown in Figure 2C. We first tested whether transferrin (Tf) internalization, a well-established clathrin-dependent endocytic process, was affected in INS-1 cells overexpressing this shRNA vector. Because the vector was tagged with EGFP, we used Tf conjugated to Alexa-568. After incubating cells with Alexa-568 Tf for 40 min, massive internalization was seen in control cells expressing the empty vector. In contrast, little cytoplasmic Tf fluorescence was observed in a cell transfected with the shRNA against clathrin (Figure 3A). After data pooling and normalization, Tf internalization in cells devoid of clathrin was quantified to be $33 \pm 0.3\%$ of the endocytosis recorded in control cells ($p < 0.001$; Figure 3B), verifying the knock-down of functional clathrin. In parallel, we showed that a knock-down of clathrin affected neither the flash-evoked exocytosis nor the subsequent excessive rapid capacitance decay ($n = 0.49$, $p = 0.70$). Instead, the slow endocytosis was selectively reduced to $24 \pm 3\%$ of the control (Figure 2D,E; $p < 0.001$). Therefore, we believe that the slow capacitance decay represents *bona fide* clathrin-dependent endocytosis.

Both fast and slow endocytosis need GTP and dynamin

Next, we examined the possible requirement of GTP in endocytosis. Replacing GTP with an equal amount of its non-hydrolyzable analog GTPγS (0.3 mM) in the pipette solution abolished both Ca^{2+}-evoked fast and slow membrane retrievals (Figure 4A; $p < 0.001$). As intracellular perfusion of GTPγS also severely compromised Ca^{2+}-evoked fusion, we used a pipette solution containing no GTP to avoid that problem. Such a treatment did not affect exocytosis but still eliminated the rapid retrieval ($29 \pm 7\%$ of the control, $p < 0.001$) and significantly inhibited the slow one as well ($61 \pm 7\%$ of the control, $p < 0.001$).

Dynamin is a guanosine triphosphatase that participates in the fission of endocytic vesicles (29). To test the role of dynamin in different modes of endocytosis, we preincubated cells in a solution containing a cell-permeable myristoylated dynamin inhibitory peptide (DIP), which effectively blocks vesicle recycling in synaptosomes (25). Preincubating cells in a DIP (50 μM)-containing solution for 20 min almost completely inhibited Ca^{2+}-evoked fast ($7 \pm 0.5\%$ of the control, $p < 0.001$) and slow ($39 \pm 4\%$ of the control, $p < 0.001$) endocytosis (Figure 4A,B). Overexpressing a dynamin mutant that was defective in GTP binding (K44E) has been shown to be effectively inhibiting endocytosis in a variety of cells (30). Because pancreatic β cells expressed both dynamin 1 (Dyn1) and dynamin 2 (Dyn2) (data not shown), we cotransfected INS-1 cells with K44E mutants of both Dyn1 and Dyn2. Overexpression of both mutants also potently reduced the fast capacitance decay ($21 \pm 4\%$ of control, $p < 0.001$), although it failed to significantly affect the slow one (Figure 4C,D), probably reflecting different requirements of fast and slow endocytosis on cytoplasmic GTP.

Figure 1: Different modulations of $[Ca^{2+}]_i$ on fast and slow endocytosis in insulin-secreting cells. A) Ca^{2+} elevation generated by uncaging of DMNP-EDTA triggered capacitance increase without decay (left), only slow (right) and both fast and slow (middle) capacitance decays after exocytosis in mouse pancreatic β cells. B) An example of Ca^{2+}-evoked fast endocytosis in INS-1 cells. The maximum rate of exocytosis, delay time for endocytosis, amplitude of total exocytosis (Exo) and endocytosis (Endo) and amplitude and time constants for fast and slow endocytosis were determined as explained in the *Materials and Methods*, and averaged data were summarized in Table 1 and Table S1. C) The relationship of maximum rate of capacitance increase and $[Ca^{2+}]_i$ in cells exhibiting fast endocytosis (circle), slow endocytosis only (downside triangle) and no endocytosis (upside triangle). The relationship between post-flash $[Ca^{2+}]_i$ and rates of exocytosis in cells exhibiting fast endocytosis could be fitted by a Hill equation (dashed line), which yielded a half-maximal $[Ca^{2+}]_i$ at 9.8 ± 1.3 μM and a coefficient of 3.5 ± 2.0. D) The rate constants for the fast process were steeply dependent on $[Ca^{2+}]_i$, which could be fitted with a Hill equation (dashed lines) with r_{max}, K_d and n as 7.8 ± 0.9 /second, 32.0 ± 3.2 μM and 4.4 ± 1.9, respectively. E) The supralinear dependence of slow endocytosis rate constants on $[Ca^{2+}]_i$ could also be described by a Hill function (dashed line) with r_{max}, K_d and n equaled to 0.6 ± 0.1 /second, 23.7 ± 2.5 μM and 7.0 ± 4.4, respectively.

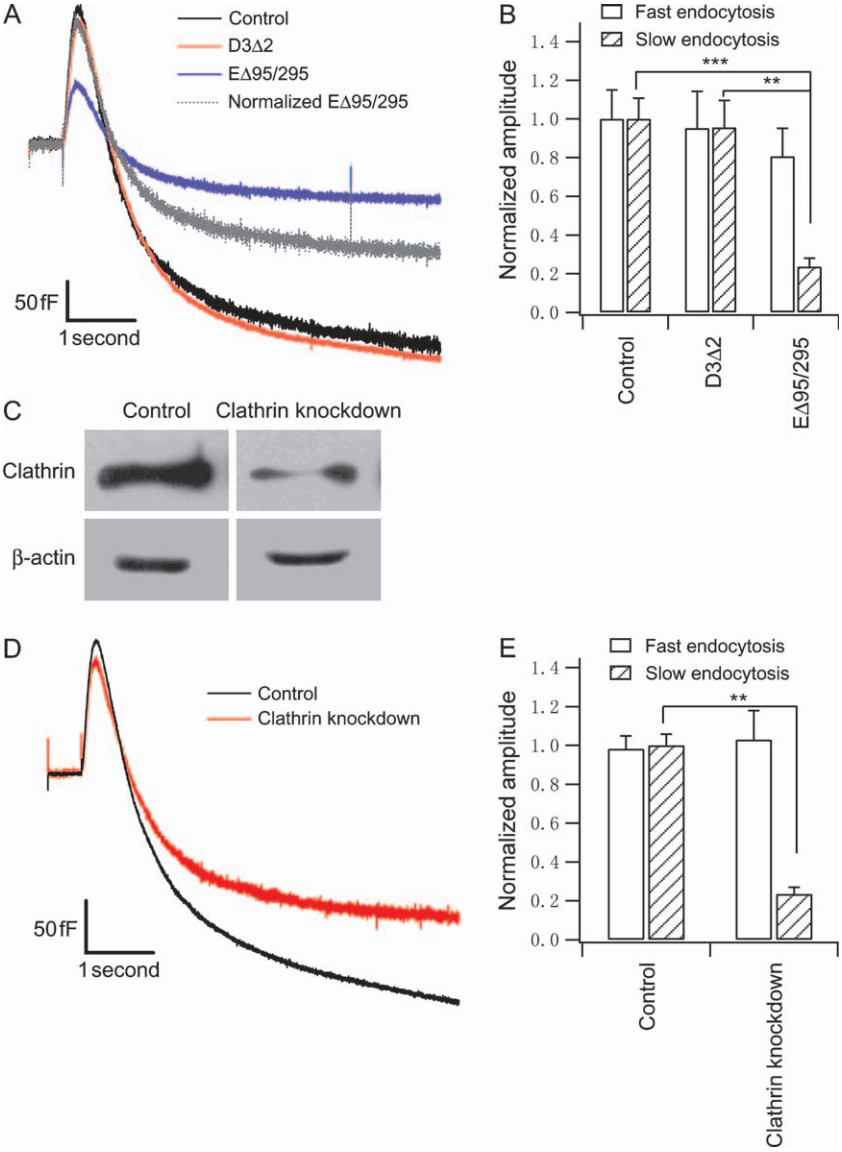

Figure 2: Perturbing clathrin-dependent pathways selectively abolishes the slow component of capacitance decay. A) Averaged Ca^{2+}-evoked capacitance dynamics in control cells (dark, $n = 39$), cells expressing control Eps15 mutant D3Δ2 (red, $n = 19$) and cells expressing dominant-negative mutant EΔ95/295 (blue, $n = 30$). Averaged capacitance trace in cells expressing EΔ95/295 mutant was normalized according to the amplitude of exocytosis in control cells and plotted as dotted gray line. B) Summary of normalized amplitude of Ca^{2+}-evoked fast and slow endocytosis in control cells and cells expressing mutants. Asterisks ** and *** that denote statistical significance are indicated on the histogram. C) Cells were transfected with the shRNA against the heavy chain of clathrin (clathrin knocking down) or the empty vector (control). Western blotting was performed on protein extracts from 10^5 cells with an antibody against the heavy chain of clathrin. An antibody against β-actin was used as a control. D) Averaged Ca^{2+}-evoked capacitance dynamics in control cells expressing the empty vector (dark, $n = 69$) and cells expressing the shRNA against the heavy chain of clathrin for 72 h (red, $n = 49$). E) Reducing endogenous clathrin significantly inhibits slow endocytosis (**$p < 0.01$, compared with control).

Nevertheless, we believe that clathrin-independent endocytosis in pancreatic β cells definitely requires GTP hydrolysis and dynamin participation.

Fast endocytosis is an actin-dependent process

Actin has been proposed to be a crucial factor in endocytosis, although its exact role is still elusive. We tried to clarify its role in our system by preincubating cells in a solution containing agents that disrupted subplasmalemmal actin networks. Because longer pretreatment with an actin depolymerization agent like cytochalasin D (cytoD) completely eliminated exocytosis as well as endocytosis (data not shown), we performed our experiments in INS-1 cells only after 20–40 min pretreatment of cytoD (20 μM). Under such circumstance, the subplasmalemmal actin networks were completed disrupted (Figure S3), while the exocytosis was not significantly affected. As shown in Figure 5A,B, fast endocytosis in cells pretreated with cytoD was inhibited to 9 ± 2% of the control, while the slow one was not significantly affected (97 ± 8% of the control). Therefore, actin polymerization may play an indispensable role in clathrin-independent endocytosis but only exerts minor effects on the clathrin-dependent one.

Clathrin-dependent and -independent endocytosis in vivo

A concern often raised is that live cells never experience UV photolysis *in vivo*. Therefore, we monitored endocytosis elicited by a physiologically relevant stimulus (70 mM KCl and 15 mM glucose) in intact cells using dual-color TIRF microscopy. By overexpressing either Dyn1–EGFP or Dyn2–EGFP with clathrin–DsRed, we could simultaneously observe the dynamics of clathrin and dynamin puncta in the resting and stimulated state. Stimulation induced a massive brightening and dimming (without diffusion) of dynamin and clathrin puncta in the subplasmalemmal

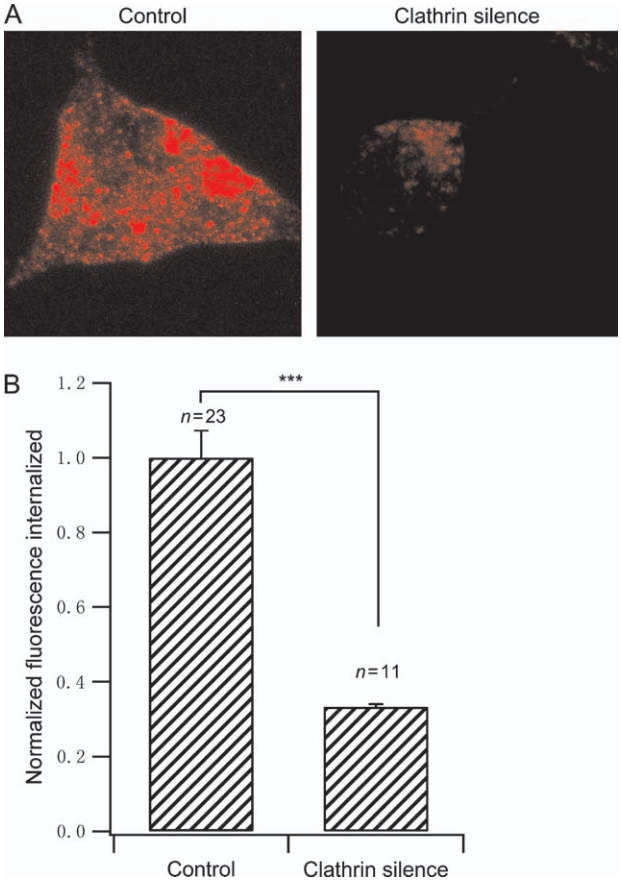

Figure 3: Inhibition of Tf internalization by clathrin knockdown in INS-1 cells. A) Control cells transfected with either the empty pRNAT-H1.1/EGFP vector (left) or the clathrin shRNA (right) were incubated in a solution containing Alexa-568 Tf (35 μg/mL) at 37°C for 40 min. Compared with control cells, internalization of Tf puncta was significantly reduced in cells transfected with the shRNA. The example images shown here were captured at the middle focal plane and were representative of at lest 11 similar cells. B) Internalized Tf fluorescence was integrated from different *z* planes, normalized to the internalization of Tf in control cells and summarized here. Asterisks *** denote statistical significance ($p < 0.001$) compared with control.

layer, which represented individual endocytic events as previously suggested (31). Clathrin and dynamin came from the cell interior to the plasma membrane and also receded together in many cases (right panel in Figure 6A), irrespective of the dynamin isoform. On the other hand, dynamin puncta also brightened and disappeared in the absence of changes in clathrin intensity, which we classified as clathrin-independent endocytic events (right panel in Figure 6B). According to that criterion, $32 \pm 4\%$ of Dyn1-dependent endocytic events were clathrin independent, which was significantly greater than the percentage of clathrin-independent endocytosis in Dyn2-transfected cells ($17 \pm 4\%$, $p < 0.01$). Interestingly, compared with that of clathrin-dependent endocytosis, the fluorescence intensity of Dyn1 was more elevated before it reached its peak during clathrin-independent endocytosis (Figure 6C), implying that different endocytosis may have different aggregating processes of dynamin.

Furthermore, in INS-1 cells coexpressing Dyn1–EGFP and clathrin–DsRed, we depolymerized cortical actin networks with cytoD (20 μM) and monitored its effects on stimulation-evoked clathrin-dependent and -independent endocytic events. On average, 8.3 ± 1.5 clathrin-independent endocytic events were observed in control cells stimulated with 70 mM KCl and 15 mM glucose for 150 seconds ($n = 10$). In consistent with electrophysiological data, actin depolymerization significantly reduced this number to 1 ± 0.3 events/cell ($n = 8$, $p < 0.001$; Figure 6D). On the other hand, the clathrin-dependent endocytosis was not significantly altered (from 17.4 ± 3.3 endocytic events per control cell to 13.8 ± 5.3 events per cell pretreated with cytoD), indicating that actin may not be required for clathrin-coated vesicle scission *per se*. However, actin disruption significantly reduced fluorescent signals of clathrin and dynamin during endocytosis and might slow down fluorescence decays from their peaks to plateaus (Figure S4), implicating a complementary role of actin. Similar phenomena were also observed in cells cotransfected with Dyn2–EGFP and clathrin–DsRed (data not shown). In summary, these results agree with the electrophysiological data and further supporting the idea that actin polymerization plays an indispensable role only in clathrin-independent endocytosis of pancreatic β cells.

The majority of clathrin-independent endocytosis in pancreatic β cells is not 'kiss and run'

'Kiss and run' of insulin-containing granules (IGs) is reported in pancreatic β cells (5), which obviously will lead to rapid retrieval of vesicle membrane. During 'kiss and run', large dense-core vesicles fuse to the plasma membrane in pancreatic β cells through a restricted fusion pore about 1.4 nm in diameter (5). If the clathrin-independent endocytosis we detected does represent 'kiss and run', we would expect to observe little stimulation-induced internalization of fluorescent dextran about 10 nm in diameter when the clathrin-dependent endocytic process is inhibited. Stimulating cells with a solution containing 70 mM KCl, 15 mM glucose and 50 μM tetramethylrhodamine dextran (70 kD) induced a massive internalization of dextran as observed under a confocal microscope (Figure 7A), which was not seen in cells preincubated in a bath solution containing only the dextran (data not shown). Preincubating cells with DIP (50 μM) almost completely abolished this internalization ($12 \pm 5\%$ of the control, $p < 0.001$), confirming the ubiquitous requirement for dynamin in both types of endocytosis (Figure 7B). To our surprise, inhibition of the clathrin-dependent pathway by overexpressing EGFP-EΔ95/295 only inhibited about $50 \pm 4\%$ of dextran internalization compared with the control cells ($p < 0.01$; Figure 7C,D). Therefore, we conclude that the majority of clathrin-independent membrane retrieval is not likely to be 'kiss and run'.

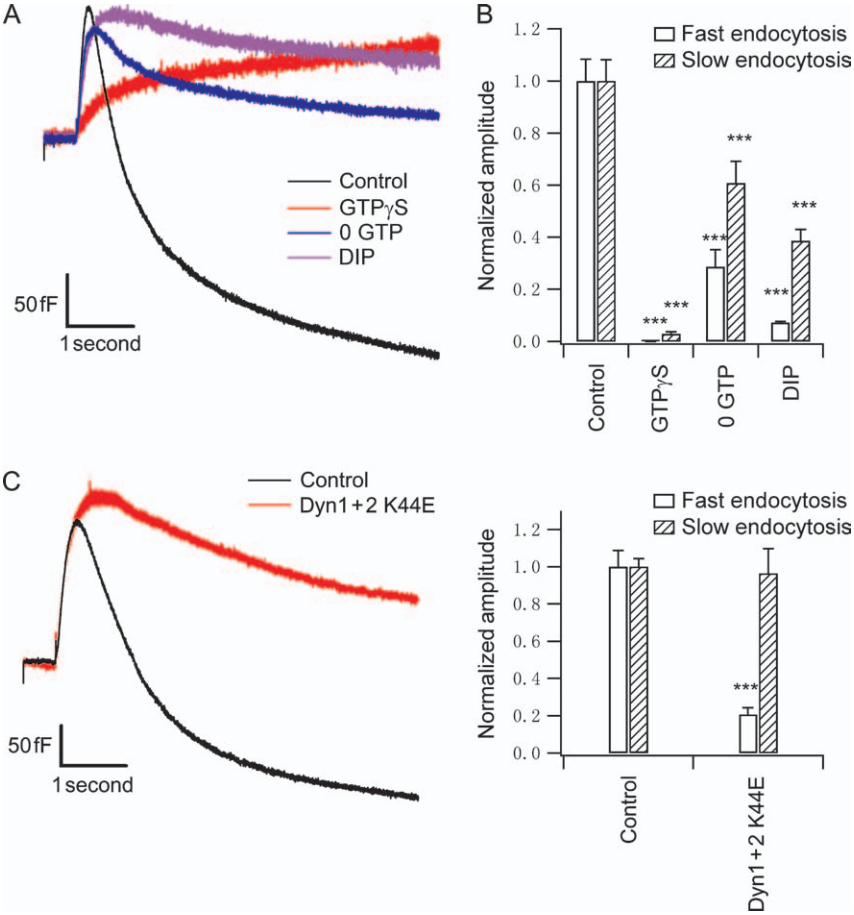

Figure 4: Requirements of GTP hydrolysis and dynamin in endocytosis. A) Averaged Ca^{2+}-evoked capacitance dynamics in control cells (dark, $n = 108$), cells intracellularly perfused with either GTPγS (0.3 mM, red, $n = 22$) or 0 GTP (blue, $n = 46$) and cells that have been pretreated with DIP for 20 min (purple, $n = 24$). B) Summary of effects on fast and slow endocytosis by treatments mentioned above. Asterisks *** denote statistical significance ($p < 0.001$) compared with control. C) Averaged Ca^{2+}-evoked capacitance dynamics in control cells (dark, $n = 83$) and cells cotransfected with Dyn1(K44E)–EGFP and Dyn2(K44E)–mRFP (red, $n = 37$). D) Summary of effects on fast and slow endocytosis by overexpressing dominant-negative dynamin mutants in INS-1 cells. Asterisks *** denote statistical significance ($p < 0.001$) compared with control.

Discussion

In this study, we observe a fast and a slow component of capacitance decay evoked by homogenous elevation in $[Ca^{2+}]_i$ in primary β cell and INS-1 cells. Replacing GTP in the pipette solution with a non-hydrolyzable analog or simply removing GTP from the pipette solution severely inhibited both types of endocytosis, similar to what has been found in chromaffin cells and neurons (4,32,33). Moreover, endocytosis was also reduced by pretreatment

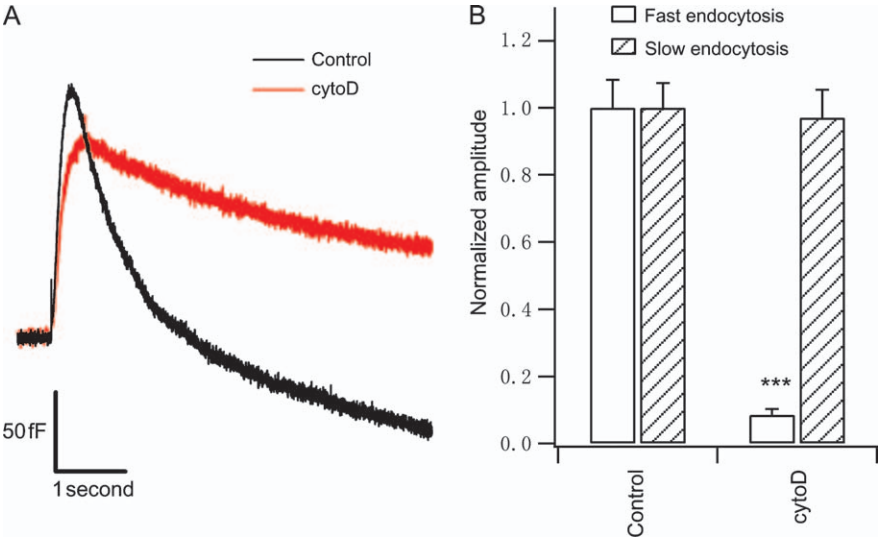

Figure 5: Actin depolymerization selectively eliminates Ca^{2+}-triggered clathrin-independent endocytosis. A) Averaged Ca^{2+}-evoked capacitance dynamics in cells pretreated with either 0.1% dimethyl sulfoxide (dark, $n = 29$) or cytoD (20 μM) (red, $n = 19$) for 20–40 min. B) Summary of effects of actin depolymerization on Ca^{2+}-evoked fast and slow endocytosis ($p < 0.001$).

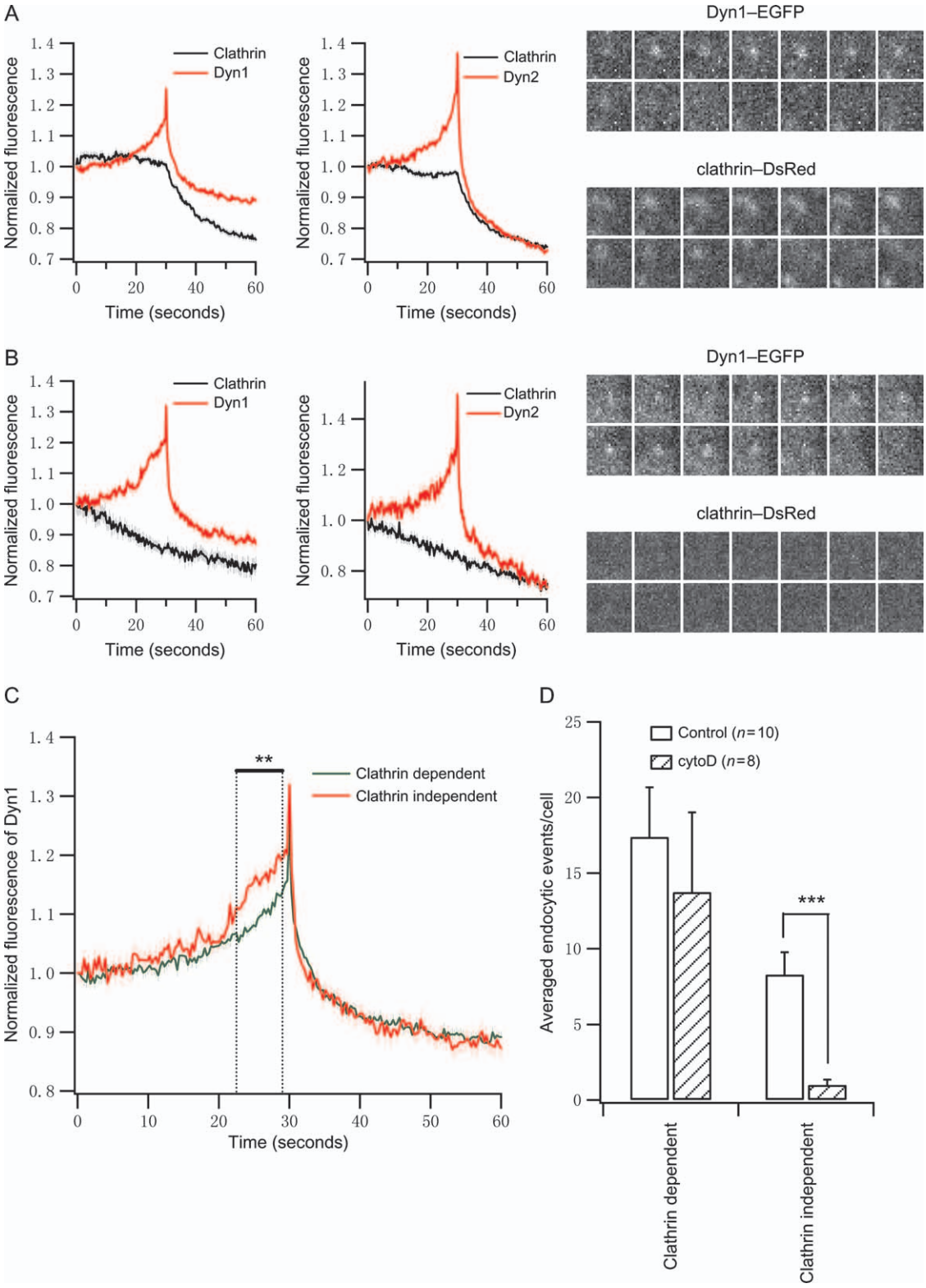

Figure 6: Legend on next page.

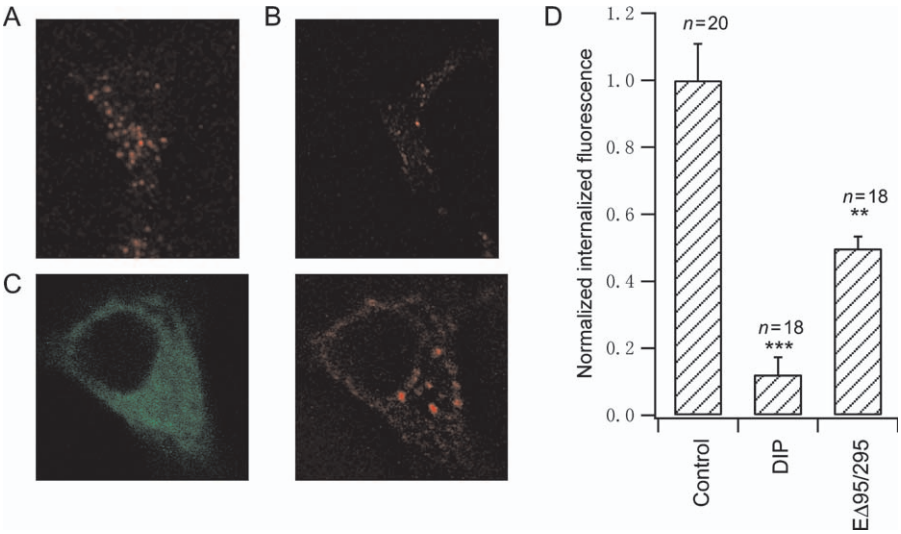

Figure 7: Inhibition of clathrin-dependent endocytosis fails to abolish internalization of high molecular weight fluorescent dextran. A) Control INS-1 cells were stimulated by a solution containing 70 mM KCl, 15 mM glucose and 70 kD tetramethylrhodamine dextran (50 μM) for 5 min, then fixed and observed under a confocal microscope, as shown by a sample image taken at the middle focal plane. B) A representative example of preincubating cells with DIP (50 μM) for 20 min almost abolished stimulation-evoked dextran internalization. C) Stimulation-triggered fluorescent dextran internalization retained in cells transfected with an EGFP-EΔ95/295 mutant. D) Summary of normalized internalization of dextran in control, DIP-treated and EΔ95/295-transfected cells. Numbers of cells tested are labeled on the graph (**$p < 0.01$, ***$p < 0.001$).

of membrane-permeable DIP. These experiments suggest that dynamin and GTP hydrolysis are general requirements for endocytosis in pancreatic β cells.

We then explored molecular identities of fast and slow membrane retrievals to address whether they were of the same identity or not. This is relevant because capacitance measurement always records a summary of exocytosis and endocytosis. Therefore, we needed to demonstrate that slow endocytosis was not merely because of contamination of fast endocytosis by simultaneous fusion of vesicles. Firstly, we showed that perturbing the clathrin-dependent pathway selectively abolished the slow capacitance decay in INS-1 cells, but spared the fast one. This was in contrast to cells that have been disrupted of cortical actin networks in which only the fast capacitance decay was blocked. In addition, we found that $[Ca^{2+}]_i$ differentially modulated fast and slow decays in capacitance. Compared with the slow decay phase, the rapid one is accelerated at higher $[Ca^{2+}]_i$ elevation (Figure 1D). As the speed of exocytosis is saturated at $[Ca^{2+}]_i$ above 20 μM (Figure 1C), which is well below the $[Ca^{2+}]_i$ range required for the acceleration of either type of capacitance decay, the relationships shown in Figure 1D are not likely to be significantly affected by simultaneous exocytosis. Therefore, we conclude that the fast and the slow capacitance decays do represent distinct endocytic processes.

Figure 6: Recruitment of both Dyn1 and Dyn2 to clathrin-dependent and -independent endocytosis *in vivo*. INS-1 cells were cotransfected with clathrin–DsRed and Dyn1–EGFP/Dyn2–EGFP. After perfusing cells with a solution containing 70 mM KCl and 15 mM glucose, rapid aggregation and disappearance of clathrin and dynamin puncta representative of individual endocytic events were observed in the subplasmalemmal plane. Fluorescence intensity was normalized to their initial resting values and aligned according to the time when dynamin puncta were maximally fluorescent. All averaged time–courses are labeled with standard error bars. A) Averaged time–courses of clathrin (dark) and Dyn1 (red)-dependent endocytic events are shown in the left panel ($n = 174$), and time–courses of clathrin (dark) and Dyn2 (red)-dependent endocytic events are shown in the middle panel ($n = 231$). Figures in the right panel show a typical example of the clathrin-dependent endocytic events observed. Appearance and disappearance of the Dyn1 puncta (top) is accompanied by similar changes in clathrin puncta (bottom). The time interval between these images is 3 seconds. B) Averaged time–courses of clathrin (dark)-independent but Dyn1 (red)-dependent endocytic events are shown in the left panel ($n = 83$), and the clathrin (dark)-independent but Dyn2 (red)-dependent ones are shown in the middle panel ($n = 44$). Similarly, figures in the right panel show a typical example of clathrin-independent but Dyn1-dependent endocytic events as Dyn1 puncta (top) appear and disappear in the absence of changes in clathrin fluorescence (bottom). C) Averaged time–courses of fluorescence fluctuations of Dyn1 in clathrin-dependent (green, $n = 174$) and clathrin-independent (red, $n = 83$) endocytosis are compared here. The two traces exhibit significant different fluorescence intensities at time interval from 22.5 to 29 seconds ($p < 0.01$). D) Preincubating cells with cytoD (20 μM) for 20 min selectively reduced the number of clathrin-independent endocytic events per cell triggered by stimulation, while failed to significantly affect the average number of clathrin-dependent events per cell. Numbers of cells tested are labeled on the graph ($p < 0.001$).

Because pancreatic β cells contain both small synaptic-like microvesicles (SVs) and IGs (34), it is possible that distinct capacitance decays simply reflect recycling of different types of vesicles. Using electron microscopy, we attempted to quantify the relative amount and size of IGs and SVs in the INS-1 cells we used. We found that an individual INS-1 cell contained about six times less SVs than IGs (409 IGs and 66 SVs from 28 different samples; Figure S5), which was in good agreement with data obtained from primary β cells previously (34,35). Moreover, by fitting the observed diameter profiles of vesicles with Gaussian distributions, we estimated average diameters of IGs and SVs to be 238 ± 4 nm ($n = 409$) and 90 ± 1 nm ($n = 66$), respectively. Given that the capacitance is linearly correlated with the surface area of the membrane, fusion of one SV with the plasma membrane would produce a capacitance increase of about 15% of that of an IG. Moreover, we consistently observed more stimulation-triggered fusion events of fluorescent-labeled IGs, compared with that of SVs in live cells using TIRF microscopy (Figure S6). Added together, these data show that the capacitance measurement mainly reflects exocytosis of IGs, which later leads to retrieval of granule membrane through different mechanisms.

It has been known for a long time that synaptic vesicles recycle in a clathrin-dependent manner (36). However, there is no definite answer to whether the clathrin-dependent pathway contributes to the Ca^{2+}-evoked membrane retrieval or to the normal vesicle recycling process in pancreatic β cells. By perfusing antibodies and domains of clathrin-interacting proteins in the pipette solution, it was concluded that slow membrane capacitance decays in bipolar neurons and chromaffin cells evoked by membrane depolarization were clathrin-dependent processes (3,4). However, intracellular perfusion of peptide may lead to effects that are not exerted by the endogenous protein (37). For example, overexpressing or intracellularly perfusing SH3–amphiphysin in chromaffin cells led to contradictory results regarding its effect on vesicle fusion pore dynamics (38,39). In addition, using TIRF microscopy, no change of clathrin puncta (EGFP was tagged to the light chain of clathrin) was observed in a mouse insulinoma cell line (MIN6) cells depolarized with 50 mM KCl, whereas significant release of neuropeptide Y (NPY) from granules and changes of Dyn1–EGFP puncta were detected (40). Therefore, we approached this problem in a different way. The slow endocytosis was inhibited by overexpressing Eps15 mutants, which was shown to be an essential component of clathrin-coated pits (27). Additionally, a knock-down of endogenous clathrin in INS-1 cells not only inhibited Tf internalization but also selectively reduced Ca^{2+}-evoked slow membrane retrieval (Figure 2). Therefore, our results are in general agreement with previous reports in other preparations in that the slow endocytosis represents *bona fide* clathrin-dependent endocytosis. We also sought to detect physiological relevant stimulation-evoked individual endocytic events in INS-1 cells using TIRF microscopy. In contrast to the report in MIN6 cells (40), we found that clathrin was recruited to and dissipated from endocytic sites in the subplasmalemmal layer, indicative of clathrin-dependent endocytic events *in vivo*. Several reasons may account for this discrepancy. Because stationary clathrin-enriched structures were observed by fluorescence microscopy and proposed functionally inactive (41), it may correspond to the large, flat clathrin arrays seen at the lower surface of adherent fibroblasts in electron micrographs (42). Overexpressing exogenous clathrin seemed to increase this non-responding population of clathrin (41). Moreover, the signal-to-noise ratio of clathrin signal was less than that of dynamin (Figure 6), which was likely to be another reason for the failure in detecting clathrin-dependent endocytic events in the previous study.

Rapid endocytosis induced by either homogenous cytoplasmic Ca^{2+} elevation or membrane depolarization was initially demonstrated in a single pituitary cell (43) and subsequently detected in other preparations, such as chromaffin cells (44,45), rat corticotrophs (26), neurons (14,46) and pancreatic β cells (21,47). Later, follow-up studies showed that GTP and dynamin but not clathrin were involved in the depolarization-triggered rapid endocytosis in adrenal chromaffin cells and bipolar cells (4,33). Our data supplement those results by showing that the excessive endocytosis evoked by homogenous $[Ca^{2+}]_i$ elevation in pancreatic β cells is also independent of clathrin. Furthermore, we showed that disruption of actin networks selectively inhibited fast endocytosis and reduced the numbers of clathrin-independent endocytic events triggered by depolarization. These experiments point out a novel and pivotal role of actin polymerization in this clathrin-independent fast endocytosis. Such a requirement of actin is similar to other types of clathrin-independent endocytosis found in non-excitable cells (48–50), indicating that it may be an evolutionarily conserved process.

An important role of actin in the clathrin-mediated endocytic process has also been proposed in yeast (51) and mammalian cells (31). In contrast to the severely compromised clathrin-dependent endocytosis by actin depolymerization in Swiss 3T3 cells (31), we found that pretreating INS-1 cells with cytoD failed to suppress stimulation-evoked clathrin-dependent endocytosis, which could possibly be caused by the different depolymerization agents used in these studies. However, the dynamics of individual dynamin and clathrin puncta were altered by cytoD pretreatment (Figure S4), which indicated a role of actin in the formation or translocation of clathrin-coated vesicles, as suggested previously (52). Therefore, we favor concepts that the actin is probably not a necessity for the scission of clathrin-coated vesicles in pancreatic β cell, but may participate in other steps of this endocytic process.

The identity of this rapid clathrin-independent endocytosis is intriguing. The 'kiss and run' of large dense-core vesicles and synaptic vesicles is demonstrated in pancreatic β cells

(5) and nerve terminals (6) by cell-attached capacitance methods. In our hands, internalization of molecules up to 10 nm in diameter persisted in cells devoid of clathrin-dependent endocytosis. This eliminates a major contribution of 'kiss and run' to the clathrin-independent endocytosis we observed. Based on their TIRF experiment, Tsuboi et al. proposed a 'cavicapture' mode of recycling of IGs in MIN6 cells in which granules stayed connected to the cell surface membrane through an enlarged fusion pore without falling into the plasmalemma (40). Alternatively, at ribbon synapses of bipolar cells and saccular hair cells, membrane is retrieved predominantly in a large endocytic structure that originates from extensive uncoated invaginations termed 'bulk retrieval' (53). Similar bulk retrieval of membrane is sometimes also observed in other conventional neurons that have been stimulated intensely and repetitively (53). Further investigation is on the way to identify which category our excess membrane retrieval falls into.

Ca^{2+} plays a pivotal role in the vesicle fusion process (54). However, the impact of Ca^{2+} on endocytosis is highly controversial as it is reported to exert inhibitory (9,10), stimulatory (13–17) or no effects on endocytosis (11). We found that pronounced $[Ca^{2+}]_i$ elevation increased the percentage of β cells exhibiting fast endocytosis, which was in line with the idea that Ca^{2+} but not Ba^{2+} was essential for the rapid endocytosis (33). Beutner et al. also showed similar findings in cochlear hair cells (14). However, they did not examine the relationship between the amplitudes of endocytosis and $[Ca^{2+}]_i$ nor did they find any correlations between rate constants for endocytosis and post-flash $[Ca^{2+}]_i$ level. In our work, higher $[Ca^{2+}]_i$ speeds up both fast and slow membrane retrieval processes. Ca^{2+} cooperativities of approximately 4 and 7 were inferred from supralinear dependences of rate constants for fast and slow endocytosis on changes in $[Ca^{2+}]_i$, indicating that both types of endocytosis are highly Ca^{2+}-regulated processes. This is in sharp contrast to negative effects of $[Ca^{2+}]_i$ on endocytosis reported in bipolar cells (9,10), which could be because of the difference in cell types. However, in previous experiments, homogenous $[Ca^{2+}]_i$ elevation was achieved either by permeablizing cells with ionophores (10) or by intracellular perfusion of Ca–EGTA solution (9), either of which would profoundly affect exocytosis and many other cellular processes. More importantly, multiple types of endocytosis exist in bipolar neurons (4,7). Therefore, it is doubtful whether the relationships obtained previously reflect the effect of $[Ca^{2+}]_i$ on the same type of endocytosis, which is solved in this study by the clean dissection of these two endocytic processes.

The clathrin-dependent endocytosis observed here is faster than depolarization-stimulated slow endocytosis reported in other excitable cells previously (2). This is probably because greater and more homogenous $[Ca^{2+}]_i$ elevation generated by flash photolysis accelerates slow endocytosis, as depicted in Figure 1E. Indeed, compared with flash photolysis, depolarization usually generated less increase in $[Ca^{2+}]_i$ and triggered a slow endocytosis with greater time constant in corticotrophs [see Figures 3 and 5 in Lee and Tse (26)].

Several laboratories working on a variety of cell types have provided evidence that prolonged or repetitive depolarization always leads to a slowing down of endocytosis, despite generation of an elevated $[Ca^{2+}]_i$ (2). Artalejo et al. proposed that sustained stimulation shifted the endocytosis from the rapid one to the slow one in chromaffin cells, but the underlying mechanism for this shift remained unknown (3). We found that an increase in $[Ca^{2+}]_i$ was linearly correlated with the amplitude of clathrin-dependent endocytosis but not the clathrin-independent one (Figure S2), implicating that the latter was of limited size. Based on these results, we hypothesize that intense stimulation may saturate the fast recycling pathway that is of limited capacity, divert the endocytosis toward the slow but relatively unlimited pathway and contribute to this phase shift. More experiments are needed to test this theory in the future. Overall, we show that multiple Ca^{2+}-sensitive processes participate in both clathrin-dependent and -independent endocytosis in pancreatic β cells. Having a clean molecular dissection, it becomes possible to identify Ca^{2+} sensors, such as synaptotagmins (55), calcineurin (25) and calmodulin (56) that are required in distinct steps of different endocytic processes. These will ultimately lead to a better understanding of both clathrin-dependent and -independent endocytosis in both excitable and non-excitable cells.

In summary, we have deciphered two types of mechanically different endocytic processes in pancreatic β cells, both of which require GTP hydrolysis and function of dynamin. The slow one is a clathrin-dependent process that could be accelerated by increase in $[Ca^{2+}]_i$. We also show that the fast one represents a novel clathrin-independent but actin-dependent bulk endocytosis and is not 'kiss and run'. Much higher $[Ca^{2+}]_i$ is required to initiate and accelerate this excessive retrieval, indicative of different Ca^{2+} sensors for the different endocytic processes.

Materials and Methods

Cell culture and transfection

β cells from 4- to 7-week-old male BALB/c mice and INS-1 insulinoma cells were isolated and cultured as described previously (57). INS-1 cells were transfected using Lipofectamine™ 2000 (Invitrogen) following the manufacturers recommendations. Forty-eight hours (for complementary DNA) or 72 h (for shRNA) after transfection, cells were detached using trypsin–EDTA and transferred onto poly-L-lysine-coated coverslips.

DNA construction and RNA interference

The clathrin–DsRed plasmid was a gift from Professor Kirchhausen (Harvard Medical School), while rat Dyn1–EGFP and Dyn2–EGFP were kindly provided by Professor McNiven (Mayo Clinic). By fusing monomeric red fluorescent protein (mRFP) to the C-terminus of Dyn2, we made a red

fluorescent version of Dyn2 K44E mutants [Dyn1(K44E)–EGFP and Dyn2(K44E)–mRFP] using QuikChange XL site-directed mutagenesis kit (Stratagene). The controlled and dominant-negative Eps15 mutants (EGFP-D3Δ2, EGFP-EΔ95/295 and EGFP-DIII) were kindly provided by Professor Benmerah and Professor Dautry-Varsat (Department of Infectious Diseases, Institut Pasteur, Paris, France).

shRNA oligonucleotides against the heavy chain of clathrin was designed and cloned into the *Bam*HI–*Hin*dIII sites of the pRNAT-H1.1/EGFP vector (58). We designed four shRNA sequences targeting the rat clathrin gene and selected the most effective one CAGAAGAATCGACGTTA by Western blotting. For Western blotting experiments, INS-1 cells were transfected with the empty vector or specific shRNAs and cultured in a solution containing G418 (100 μg/mL). After selection for a week, more than 90% of the cells positively expressed the specific vector and were subsequently collected for antibody labeling. Antibody used was mouse monoclonal antibody against the heavy chain of clathrin (BD Pharmingen) in a diluted form (1:500). β-actin antibody (Sigma; 1:2000) was used as a control. Incubation with mouse antibody was followed by application of rabbit anti-mouse immunoglobulin G peroxidase conjugate (Sigma; 1:1000). The blots were then probed with SuperSignal West Pico Chemiluminescent Substrate (PIERCE).

Electrophysiology and capacitance analysis

Electrophysiological experiments were conducted with standard whole-cell recordings using an EPC-10 patch-clamp amplifier (HEKA). Extracellular solution contained NaCl 130 mM, KCl 2.8 mM, $MgCl_2$ 1.2 mM, Glucose 5 mM, HEPES 10 mM, tetraethyl-ammonium chloride (TEA-Cl) 20 mM and $CaCl_2$ 2.6 mM with pH 7.2. The whole-cell pipette solution contained CsGlu 110 mM, DMNP-EDTA 5 mM (7 mM in high Ca^{2+} experiments), NaCl 8 mM, $CaCl_2$ 3.6 mM, MgATP 2 mM, GTP 0.3 mM, HEPES 37 mM and fura-6F or mag-fura2 0.2 mM (in high Ca^{2+} experiments) with pH adjusted to 7.2 using CsOH or HCl. Flash photolysis and increase in membrane capacitance were performed as described previously (57).

Capacitance traces were analyzed in detail as shown in Figure 1B. As exocytosis was frequently accompanied by subsequent endocytosis, we fitted the initial capacitance increase with a dashed line to obtain the initial rate (also the maximal rate) of exocytosis. The total exocytosis was measured as the difference between the amplitude of capacitance at the peak reached within the recording time and the amplitude of capacitance before stimulation. The total endocytosis was measured as the result of the amplitude of maximum capacitance minus the minimal one. The delay time for the endocytosis (t_1) was defined as the time interval between the UV photolysis and the appearance of capacitance decay. The capacitance decay was fitted with either a single exponential function, $f(t) = A_0 - A_1 \times \{1 - \exp[-(t - \tau_0)/\tau_1]\}$, or a double exponential function, $f(t) = A_0 - A_1 \times \{1 - \exp[-(t - \tau_0)/\tau_1]\} - A_2 \times \{1 - \exp[-(t - \tau_0)/\tau_2]\}$, depending on the best quality of the fit. A_1 and A_2 represented amplitudes of the fast and the slow components, while τ_1 and τ_2 were time constants. The rate constants for fast and slow membrane retrievals were obtained as $r_1 = 1/\tau_1$ and $r_2 = 1/\tau_2$, respectively. The correlations between endocytic rate constants and $[Ca^{2+}]_i$ were fitted with Hill equation

$$r = r_0 + \frac{r_{max} - r_0}{1 + \left(\frac{K_d}{[Ca^{2+}]_i}\right)^n}$$

in which $[Ca^{2+}]_i$ was measured at the time when endocytosis started. To exclude impact of different exocytosis on endocytosis, amplitudes of both fast and slow endocytosis were first divided by amplitudes of the preceding exocytosis in the same cells, then normalized to the averaged value in the control cells and summarized as histograms later.

Confocal and TIRF microscopy

For the dextran internalization experiment, INS-1 cells were stimulated with tetramethylrhodamine dextran (70 kD, 50 μM) combined in a high K^+ solution (containing NaCl 57.8 mM, KCl 70 mM, $MgCl_2$ 1.2 mM, glucose 15 mM, HEPES 10 mM and $CaCl_2$ 2.6 mM) for 5 min. To measure Tf internalization, control cells and cells transfected with shRNA against the rat clathrin were bathed in a normal solution containing Alexa 568-conjugated Tf (35 μg/mL) at 37°C for 40 min. All cells were subsequently rinsed, fixed and observed under a confocal microscope (Fluoview500; Olympus). The fluorescence of internalized puncta from different Z sections were integrated in IMAGEJ (National Institutes of Health) as described previously (57) and normalized to the signal obtained in control cells.

TIRF microscopy was conducted as described previously (57). In brief, we used a 488 nm laser to simultaneously excite EGFP and DsRed, and images were collected (3.3 Hz) and analyzed in Tillvision (TILL photonics). All endocytic events were identified manually. Some fluorescence puncta disappeared from TIRF zone when the neighboring puncta retained their position at the same time. We selected only those events to avoid artifacts introduced by changes in focus, and puncta with extensive lateral movement were also excluded from analysis. A circle of 5 pixels (335 nm) in diameter enclosing a single endocytic event was selected to calculate the averaged fluorescent signals of dynamin and clathrin. All clathrin and dynamin fluorescence was normalized to their initial resting values thereafter and aligned according to the time when the dynamin puncta was maximally fluorescent.

Data analysis

All data were analyzed using IGOR PRO software (Wavemetrics). Averaged results were presented as the mean value ± SEM with the number of experiments indicated. Statistical significance was evaluated using Student's *t*-test, and asterisks *, ** and *** denote statistical significance with p values less than 0.05, 0.01 and 0.001, respectively. In Figure S2, the linear correlation coefficient (r) and its error were calculated from the raw data using the StatsLinearCorrelationTest function from IGOR PRO in which an r value larger than zero indicated a positive correlation.

Acknowledgments

We would like to thank Professors Bertil Hille, Donner Babcock and Nathalie Sauvonnet for critical manuscript revision, Professor McNiven for providing dynamin 1 and 2 EGFP vectors, Professor Kirchhausen for the clathrin–DsRed vector and helpful discussion and Professors Dautry-Varsat and Benmerah for dominant-negative Eps15 mutants. We thank Yong Yu and Xiaoqing Yu for help with confocal microscopy. We thank Lei Sun for her help on using the electron microscope. This work was supported by grants from the National Science Foundation of China (30400157, 30670503, 30670504, 30630020 and 30611120531), grant from the Beijing Municipal Science & Technology Commission (5072034) and the Major State Basic Research Program of China (2004CB720000 and 2006CB70570).

Supplementary Materials

Supplementary Methods

Ca^{2+} photometry

Electron microscopy

Supplementary Discussion

Fast endocytosis is not affected by exocytosis

Endocytic events observed under the TIRF microscope mainly reflect retrieval of pre-fused IGs

Figure S1: Glucose-induced Ca^{2+} oscillation in INS-1 cells. INS-1 cells were loaded with fura-2/AM. After elevating the glucose level in the bath solution to 30 mM, INS-1 cells exhibited an increase in $[Ca^{2+}]_i$ and $[Ca^{2+}]_i$ oscillations. The experiment shown here is a representative of five identical experiments.

Figure S2: Both fast and slow membrane retrievals are coupled to the preceding fusion. A) The amplitudes of fast endocytosis were linearly correlated with the amplitudes of precedent exocytosis in the same cells (slope at 2.7 ± 0.3, $r_{fast} = 0.26 \pm 0.07$, $p < 0.001$, left panel). No obvious relationship was found between the pooled amplitude of the fast endocytosis and the increase in $[Ca^{2+}]_i$ (right panel). B) The amplitudes of slow endocytosis were linearly correlated with the amplitude of precedent exocytosis (slope at 1.1 ± 0.1, $r_{slow} = 0.25 \pm 0.07$, $p < 0.001$, left panel). Moreover, the averaged amplitude of slow endocytosis also exhibited linear correlation with $[Ca^{2+}]_i$ elevation (slope at 2.9 ± 0.8 pF/μM, right panel). The solid lines represent $y = 2.6 \times x$ (A) and $y = 1.06 \times x$ (B).

Figure S3: Distribution of subplasmalemmal actin networks under different situations. INS-1 cells were transfected with EGFP–actin and were imaged at the middle plane using confocal microscopy. A sample image representative of at least five similar experiments was shown in the left panel, and the right panels show spatial profiles of fluorescence intensity of EGFP along the lines imposed on the images. A subplasmalemmal actin network was found in control cell (A) but was absent in cells that had been pretreated with cytoD (20 μM) for 20 min (B).

Figure S4: Altered dynamics of dynamin and clathrin puncta during endocytosis in cells depolymerized of actin. A) Averaged time–course of clathrin (dark) and Dyn1 (red)-dependent endocytic events in cells pretreated with cytoD (20 μM) for 20 min (solid line, $n = 110$) and in control cells (dashed line, $n = 174$). Compared with untreated cells, averaged decays of Dyn1 and clathrin fluorescence from their peaks to basal levels were apparently reduced in amplitude and speed in cells pretreated with cytoD. B) Summary of decreases in the fluorescence intensities of clathrin and Dyn1 during the later stage of endocytosis in control cells and cells pretreated with cytoD, which were calculated as the difference between averaged fluorescence intensities at time interval 30–32 and 50–55 seconds, as depicted in (A).

Figure S5: IGs and small SVs in INS-1 cells. A) An electron micrograph of an INS-1 cell containing both dense-core IGs and clear SVs (arrowhead), which is representative of 28 similar images. B) The distribution of the diameters of IGs was fitted with a single Gaussian distribution (dotted line), yielded a mean diameter of 238 ± 4 nm. C) The distribution of the diameters of SVs was fitted with a single Gaussian distribution (dotted line), yielded a mean diameter of 90 ± 1 nm.

Figure S6: IGs and SVs in live cells. A) A INS-1 cell was cotransfected with vesicular acetylcholine transporter (vAcht)-EGFP and NPY-DsRed and was observed under a TIRF microscope. The image shown here represents six similar experiments. B) After stimulating INS-1 cells with 70 mM KCl and 15 mM glucose, fusions of IGs and SVs to the plasma membrane under the TIRF microscope were determined and counted manually as reported previously (S5). The total numbers of the fusion events were then divided by the total recording time and the surface area of the cell, which yielded fusion frequencies of IGs and SVs of that cell. The averaged fusion frequencies of IGs and SVs are shown here ($n = 6$).

Table S1: Ca^{2+}-evoked capacitance changes are sorted based on the ratio of the amplitude of endocytosis to exocytosis. All data are averaged values

Supplemental materials are available as part of the online article at http://www.blackwell-synergy.com

References

1. Harata NC, Aravanis AM, Tsien RW. Kiss-and-run and full-collapse fusion as modes of exo-endocytosis in neurosecretion. J Neurochem 2006;97:1546–1570.
2. Royle SJ, Lagnado L. Endocytosis at the synaptic terminal. J Physiol 2003;553:345–355.
3. Artalejo CR, Elhamdani A, Palfrey HC. Sustained stimulation shifts the mechanism of endocytosis from dynamin-1-dependent rapid endocytosis to clathrin- and dynamin-2-mediated slow endocytosis in chromaffin cells. Proc Natl Acad Sci U S A 2002;99:6358–6363.
4. Jockusch WJ, Praefcke GJ, McMahon HT, Lagnado L. Clathrin-dependent and clathrin-independent retrieval of synaptic vesicles in retinal bipolar cells. Neuron 2005;46:869–878.
5. Macdonald PE, Braun M, Galvanovskis J, Rorsman P. Release of small transmitters through kiss-and-run fusion pores in rat pancreatic beta cells. Cell Metab 2006;4:283–290.
6. He L, Wu XS, Mohan R, Wu LG. Two modes of fusion pore opening revealed by cell-attached recordings at a synapse. Nature 2006;444:102–105.
7. Holt M, Cooke A, Wu MM, Lagnado L. Bulk membrane retrieval in the synaptic terminal of retinal bipolar cells. J Neurosci 2003;23:1329–1339.
8. Paillart C, Li J, Matthews G, Sterling P. Endocytosis and vesicle recycling at a ribbon synapse. J Neurosci 2003;23:4092–4099.
9. von Gersdorff H, Matthews G. Inhibition of endocytosis by elevated internal calcium in a synaptic terminal. Nature 1994;370:652–655.
10. Rouze NC, Schwartz EA. Continuous and transient vesicle cycling at a ribbon synapse. J Neurosci 1998;18:8614–8624.
11. Wu LG, Betz WJ. Nerve activity but not intracellular calcium determines the time course of endocytosis at the frog neuromuscular junction. Neuron 1996;17:769–779.
12. Neves G, Gomis A, Lagnado L. Calcium influx selects the fast mode of endocytosis in the synaptic terminal of retinal bipolar cells. Proc Natl Acad Sci U S A 2001;98:15282–15287.
13. Wu W, Xu J, Wu XS, Wu LG. Activity-dependent acceleration of endocytosis at a central synapse. J Neurosci 2005;25:11676–11683.
14. Beutner D, Voets T, Neher E, Moser T. Calcium dependence of exocytosis and endocytosis at the cochlear inner hair cell afferent synapse. Neuron 2001;29:681–690.
15. Klingauf J, Kavalali ET, Tsien RW. Kinetics and regulation of fast endocytosis at hippocampal synapses. Nature 1998;394:581–585.
16. Sankaranarayanan S, Ryan TA. Calcium accelerates endocytosis of vSNAREs at hippocampal synapses. Nat Neurosci 2001;4:129–136.
17. Ales E, Tabares L, Poyato JM, Valero V, Lindau M, Alvarez de Toledo G. High calcium concentrations shift the mode of exocytosis to the kiss-and-run mechanism. Nat Cell Biol 1999;1:40–44.
18. Lindau M, Neher E. Patch-clamp techniques for time-resolved capacitance measurements in single cells. Pflugers Arch 1988;411:137–146.
19. Kanno T, Ma X, Barg S, Eliasson L, Galvanovskis J, Gopel S, Larsson M, Renstrom E, Rorsman P. Large dense-core vesicle exocytosis in pancreatic beta-cells monitored by capacitance measurements. Methods 2004;33:302–311.
20. Rorsman P, Eliasson L, Renstrom E, Gromada J, Barg S, Gopel S. The cell physiology of biphasic insulin secretion. News Physiol Sci 2000;15:72–77.
21. Eliasson L, Proks P, Ammala C, Ashcroft FM, Bokvist K, Renstrom E, Rorsman P, Smith PA. Endocytosis of secretory granules in mouse pancreatic beta-cells evoked by transient elevation of cytosolic calcium. J Physiol 1996;493:755–767.
22. Gromada J, Bokvist K, Ding WG, Barg S, Buschard K, Renstrom E, Rorsman P. Adrenaline stimulates glucagon secretion in pancreatic A-cells by increasing the Ca2+ current and the number of granules close to the L-type Ca2+ channels. J Gen Physiol 1997;110:217–228.
23. James Keener JS. Mathematical Physiology. New York: Springer-Verlag; 1998.
24. Engisch KL, Nowycky MC. Compensatory and excess retrieval: two types of endocytosis following single step depolarizations in bovine adrenal chromaffin cells. J Physiol 1998;506:591–608.

25. Marks B, McMahon HT. Calcium triggers calcineurin-dependent synaptic vesicle recycling in mammalian nerve terminals. Curr Biol 1998;8: 740–749.
26. Lee AK, Tse A. Endocytosis in identified rat corticotrophs. J Physiol 2001;533:389–405.
27. Morgan JR, Prasad K, Jin S, Augustine GJ, Lafer EM. Eps15 homology domain-NPF motif interactions regulate clathrin coat assembly during synaptic vesicle recycling. J Biol Chem 2003;278:33583–33592.
28. Benmerah A, Poupon V, Cerf-Bensussan N, Dautry-Varsat A. Mapping of Eps15 domains involved in its targeting to clathrin-coated pits. J Biol Chem 2000;275:3288–3295.
29. Cao H, Garcia F, McNiven MA. Differential distribution of dynamin isoforms in mammalian cells. Mol Biol Cell 1998;9:2595–2609.
30. Hinshaw JE. Dynamin and its role in membrane fission. Annu Rev Cell Dev Biol 2000;16:483–519.
31. Merrifield CJ, Perrais D, Zenisek D. Coupling between clathrin-coated-pit invagination, cortactin recruitment, and membrane scission observed in live cells. Cell 2005;121:593–606.
32. Yamashita T, Hige T, Takahashi T. Vesicle endocytosis requires dynamin-dependent GTP hydrolysis at a fast CNS synapse. Science 2005;307:124–127.
33. Artalejo CR, Henley JR, McNiven MA, Palfrey HC. Rapid endocytosis coupled to exocytosis in adrenal chromaffin cells involves Ca2+, GTP, and dynamin but not clathrin. Proc Natl Acad Sci U S A 1995;92: 8328–8332.
34. MacDonald PE, Obermuller S, Vikman J, Galvanovskis J, Rorsman P, Eliasson L. Regulated exocytosis and kiss-and-run of synaptic-like microvesicles in INS-1 and primary rat beta-cells. Diabetes 2005;54: 736–743.
35. Braun M, Wendt A, Birnir B, Broman J, Eliasson L, Galvanovskis J, Gromada J, Mulder H, Rorsman P. Regulated exocytosis of GABA-containing synaptic-like microvesicles in pancreatic beta-cells. J Gen Physiol 2004;123:191–204.
36. Heuser JE, Reese TS. Evidence for recycling of synaptic vesicle membrane during transmitter release at the frog neuromuscular junction. J Cell Biol 1973;57:315–344.
37. Anggono V, Smillie KJ, Graham ME, Valova VA, Cousin MA, Robinson PJ. Syndapin I is the phosphorylation-regulated dynamin I partner in synaptic vesicle endocytosis. Nat Neurosci 2006;9:752–760.
38. Elhamdani A, Azizi F, Solomaha E, Palfrey HC, Artalejo CR. Two mechanistically distinct forms of endocytosis in adrenal chromaffin cells: differential effects of SH3 domains and amphiphysin antagonism. FEBS Lett 2006;580:3263–3269.
39. Graham ME, O'Callaghan DW, McMahon HT, Burgoyne RD. Dynamin-dependent and dynamin-independent processes contribute to the regulation of single vesicle release kinetics and quantal size. Proc Natl Acad Sci U S A 2002;99:7124–7129.
40. Tsuboi T, McMahon HT, Rutter GA. Mechanisms of dense core vesicle recapture following ''kiss and run'' (''cavicapture'') exocytosis in insulin-secreting cells. J Biol Chem 2004;279:47115–47124.
41. Ehrlich M, Boll W, Van Oijen A, Hariharan R, Chandran K, Nibert ML, Kirchhausen T. Endocytosis by random initiation and stabilization of clathrin-coated pits. Cell 2004;118:591–605.
42. Heuser JE, Kirschner MW. Filament organization revealed in platinum replicas of freeze-dried cytoskeletons. J Cell Biol 1980;86:212–234.
43. Thomas P, Lee AK, Wong JG, Almers W. A triggered mechanism retrieves membrane in seconds after Ca(2+)-stimulated exocytosis in single pituitary cells. J Cell Biol 1994;124:667–675.
44. Heinemann C, Chow RH, Neher E, Zucker RS. Kinetics of the secretory response in bovine chromaffin cells following flash photolysis of caged Ca2+. Biophys J 1994;67:2546–2557.
45. Smith C, Neher E. Multiple forms of endocytosis in bovine adrenal chromaffin cells. J Cell Biol 1997;139:885–894.
46. Hsu SF, Jackson MB. Rapid exocytosis and endocytosis in nerve terminals of the rat posterior pituitary. J Physiol 1996;494:539–553.
47. Takahashi N, Kadowaki T, Yazaki Y, Miyashita Y, Kasai H. Multiple exocytotic pathways in pancreatic beta cells. J Cell Biol 1997;138:55–64.
48. Conner SD, Schmid SL. Regulated portals of entry into the cell. Nature 2003;422:37–44.
49. Sauvonnet N, Dujeancourt A, Dautry-Varsat A. Cortactin and dynamin are required for the clathrin-independent endocytosis of gammac cytokine receptor. J Cell Biol 2005;168:155–163.
50. Pelkmans L, Puntener D, Helenius A. Local actin polymerization and dynamin recruitment in SV40-induced internalization of caveolae. Science 2002;296:535–539.
51. Kaksonen M, Toret CP, Drubin DG. A modular design for the clathrin- and actin-mediated endocytosis machinery. Cell 2005;123:305–320.
52. Yarar D, Waterman-Storer CM, Schmid SL. A dynamic actin cytoskeleton functions at multiple stages of clathrin-mediated endocytosis. Mol Biol Cell 2005;16:964–975.
53. Logiudice L, Matthews G. Endocytosis at ribbon synapses. Traffic 2007; 9:1123–1128.
54. Sudhof TC. The synaptic vesicle cycle. Annu Rev Neurosci 2004;27: 509–547.
55. Wu LG. Kinetic regulation of vesicle endocytosis at synapses. Trends Neurosci 2004;27:548–554.
56. Artalejo CR, Elhamdani A, Palfrey HC. Calmodulin is the divalent cation receptor for rapid endocytosis, but not exocytosis, in adrenal chromaffin cells. Neuron 1996;16:195–205.
57. Duman JG, Chen L, Palmer AE, Hille B. Contributions of intracellular compartments to calcium dynamics: implicating an acidic store. Traffic 2006;7:859–872.
58. Yang X, Xu P, Xiao Y, Xiong X, Xu T. Domain requirement for the membrane trafficking and targeting of syntaxin 1A. J Biol Chem 2006; 281:15457–15463.